

# We are IntechOpen, the world's leading publisher of Open Access books Built by scientists, for scientists

6,900

Open access books available

186,000

International authors and editors

200M

Downloads

Our authors are among the

154

Countries delivered to

TOP 1%

most cited scientists

12.2%

Contributors from top 500 universities



WEB OF SCIENCE™

Selection of our books indexed in the Book Citation Index  
in Web of Science™ Core Collection (BKCI)

Interested in publishing with us?  
Contact [book.department@intechopen.com](mailto:book.department@intechopen.com)

Numbers displayed above are based on latest data collected.  
For more information visit [www.intechopen.com](http://www.intechopen.com)



# Tensile Properties in $\beta$ -Modified Isotactic Polypropylene

*Koh-hei Nitta and Tsutomu Takashima*

## Abstract

Spherulitic isotactic polypropylenes (iPPs) having a wide range of  $\beta$ -phase contents were prepared by adding  $\beta$ -nucleators, and the effects of the  $\beta$ -phase modification on the mechanical properties of the iPP were investigated. This chapter described the tensile properties of  $\beta$ -nucleated iPP, while key structural parameters, such as spherulite size and crystallinity, were controlled. The increase in the  $\beta$ -phase content led to broader yield peaks and an enhancement in the yield toughness but to a reduction in the yield strength. On the other hand, the initial elastic modulus was found to be independent of the  $\beta$ -contents. Furthermore, the deformation of the  $\beta$ -spherulites, which have a sheaflike structure, was anisotropic and depended on the stretching direction with respect to the sheaf axis. Consequently, the improved drawability and ductility of  $\beta$ -iPP compared to  $\alpha$ -iPP are thus associated with the enhanced toughness resulting from the multiple deformation processes in the sheaflike spherulites.

**Keywords:**  $\beta$ -phase crystal, mechanical properties, tensile deformation, spherulite, crystalline morphology

## 1. Introduction

As well-known, isotactic polypropylene (iPP) is a polymorphic material with various crystal forms [1], such as monoclinic ( $\alpha$ ), hexagonal ( $\beta$ ), triclinic ( $\gamma$ ), and smectic, of which the  $\alpha$ -phase is the most typical crystalline form. Commercial grades of iPP usually crystallize into the  $\alpha$ -phase with sporadic occurrence of the  $\beta$ -phase under higher supercooling [2]. Crystallization under a temperature gradient [3] or flow-induced crystallization [4, 5] encourages the formation of the  $\beta$ -phase. To prepare of  $\beta$ -modified iPP samples, the introduction of selective  $\beta$ -nucleators is the most reliable method [6]. However, unless using specific  $\beta$ -nucleating agents, the  $\beta$ -phase cannot be obtained at high levels and is always accompanied by  $\alpha$ -phase crystals. The  $\alpha/\beta$  ratio is very sensitive to the crystallization temperature and the cooling rate because of the different nucleation rates of the two crystalline species. Varga et al. [7] found that pure  $\beta$ -phase can be achieved in the presence of some selective  $\beta$ -nucleators by the selection of appropriate thermal conditions for crystallization. Furthermore, the  $\beta$ -phase was found to be transformed to the  $\alpha$ -phase by heat treatment [8]. This demonstrates that the monoclinic structure is thermodynamically stable, whereas the hexagonal  $\beta$ -phase is metastable and difficult to obtain under normal processing conditions.

Recently the number of practical studies has increased [9] because the impact strength and toughness of  $\beta$ -nucleated iPP exceed those of  $\alpha$ -iPP. Although many studies have compared the mechanical properties of  $\alpha$ -iPP and  $\beta$ -iPP, the morphological origin of the differences in the mechanical properties has not been clarified yet.

The mechanical properties of semicrystalline polymers such as iPP and polyethylene (PE) are governed by their morphological features which are specified by several structural variables such as the degree of crystallinity, spherulite size, crystalline thickness, and structural organization of the supermolecular structure [10]. These diversity and independencies of these structural variables make it difficult to provide a molecular or structural interpretation for the mechanical properties and deformation behavior of semicrystalline polymers [10]. Indeed, changing the thermal or processing conditions involves the concomitant modification of several structural parameters; thus, it is difficult to determine the structural origin of the change in mechanical properties as reported by Labour et al. [11]. Consequently, it is necessary to keep all the other structural parameters to be fixed to elucidate the effects of a given structural parameter on the mechanical properties. Very few studies have dealt with the mechanical properties of  $\beta$ -nucleated iPP with a wide range of  $\beta$ -phase contents, while all the other structural parameters, such as supermolecular organization and crystallinity, are controlled. The aim of this chapter is to elucidate the influence of the  $\beta$ -phase modification on the tensile properties of iPP. For this purpose, crystallization procedures, for the production of iPP sheets having a wide range of  $\beta$ -phase contents with fixed crystallinity and spherulite size, were developed. In addition, the effects of spherulitic morphology on tensile properties were investigated by comparing the differences in deformation mechanism of isolated  $\alpha$ - and  $\beta$ -spherulites.

## **2. Structural characterization of $\beta$ -modified isotactic polypropylene**

### **2.1 Preparation method of $\beta$ -modified polypropylene sheets**

The starting material was a commercial iPP with a high tacticity (98%) obtained in powder form. The weight-averaged molecular weight  $M_w$  and polydispersity index  $M_w/M_n$  determined by gel permeation chromatography were  $204 \times 10^3$  and 6.2, respectively. A  $\beta$ -nucleator prepared from an alcohol solution of pimelic acid and calcium stearate was used. The iPP powder was added to the solution, and it was dried in an oven at 373 K for 90 min.

The  $\beta$ -nucleator-added iPP powder was pressed and melted at 483 K. The samples were completely melted for 5 min between two aluminum plates prior to the application of 7.8 MPa pressure to produce specimens of approximately 0.2 mm thick. Adjustment of the degree of crystallinity in the volume fraction and the spherulite size to the same value for all the samples was made by changing the quenching temperature and the amount of the  $\beta$ -nucleators. The molten samples were allowed to equilibrate under pressure for 5 min prior to cooling. On removal from the press, the samples were plunged directly into a water bath maintained at an appropriate temperature 0, 30, 60, and 100°C and subsequently tempered for various periods at 100°C. Consequently, these procedures enabled us to achieve sample specimens having a wide range of  $\beta$ -phase contents with a constant crystallinity of about 65% and spherulite radius  $R$  of around 4  $\mu\text{m}$ . The structural and morphological characteristics of the samples were summarized in **Table 1**. The end numeral of the sample code PP denotes the  $\beta$ -phase concentration in the crystalline

Sample	$\beta$ -Cont. / %	$\rho_c / \text{kg m}^{-3}$	$\rho / \text{kg m}^{-3}$	$\chi_v / \%$	R / $\mu\text{m}$
PP0	0	936.0	908	65.9	3.6
PP16	16.4	933.5	906	65.3	3.7
PP43	42.7	929.6	904	66.1	4.3
PP65	65.4	926.2	901	65.1	5.1
PP83	83.0	923.5	900	66.1	4.9
PP98	97.8	921.3	898	65.3	4.4

**Table 1.**  
 Characteristics of iPP sheets.

fraction of the iPP. In this chapter, PP0 is denoted by  $\alpha$ -iPP and PP98 is denoted by  $\beta$ -iPP.

The crystalline  $\beta$ -phase content (the volume fraction of the  $\beta$ -phase in the crystalline portion) was determined from WAXD patterns. The WAXD measurements were carried out at room temperature with a Rigaku RU-200 diffractometer with Ni-filtered Cu-K $\alpha$  radiation from a generator operated at 40 kV and 100 mA. The  $\beta$ -phase fraction in the crystalline part of the specimens was assessed from the ratio of the area of the main (300)  $\beta$ -phase to the sum of the areas of the four main crystalline reflections: (110), (040), and (130) from the  $\alpha$ -phase plus (300) from the  $\beta$ -phase using Turner-Jones method [12].

Here, we modified the analysis method proposed by Somani et al. [13] to obtain the volume fraction of  $\beta$ -phase in the crystalline fraction quantitatively. The reflection peaks in the WAXD profiles were deconvoluted. In the WAXD profile, (110) at 14.1°, (040) at 16.9°, and (130) at 18.5° are the principal reflections (in  $2\theta$ ) of the  $\alpha$ -phase crystals of iPP, whereas (300) at 16.1° is the principal reflection of  $\beta$ -phase crystals, and are considered as the markers for  $\alpha$ -phase and  $\beta$ -phase crystals, respectively. The various reflection areas were computed after subtraction of the amorphous halo.

The volume fraction of  $\beta$ -phase crystals was calculated using the following equations:

$$\phi_\beta = \frac{S_{\beta(300)}\rho_{\beta c}^{-1}}{S_{\beta(300)}\rho_{\beta c}^{-1} + kS_{\alpha}\rho_{\alpha c}^{-1}} \quad (1)$$

and

$$S_\alpha = S_{\alpha(110)} + S_{\alpha(040)} + S_{\alpha(130)} \quad (2)$$

Here  $k$  is the calibration factor,  $\rho_{\beta c}$  ( $=921 \text{ kg m}^{-3}$ ) is the density of the  $\beta$ -phase crystal [14–16],  $\rho_{\alpha c}$  ( $=936 \text{ kg m}^{-3}$ ) is the density of  $\alpha$ -phase crystal [17],  $S_\beta$  is the area of the (300) reflection peak, and  $S_\alpha$  is the sum of the areas of (110), (040), and (130) peaks of  $\alpha$ -phase crystals, respectively. The calibration constant  $k$  was estimated to be 1.11 from the difference in the sensitivity of WAXD reflections with respect to the thickness of the sheets for the  $\alpha$ -phase and  $\beta$ -phase reflections.

Crystallinity can be precisely determined from density data. The densities of the specimens were determined by the flotation method. A binary medium prepared from various ratios of distilled water and ethanol was used. The volume crystallinity can be obtained using

$$\chi_V = \frac{\rho - \rho_a}{\rho_c - \rho_a} \quad (3)$$

where  $\rho$  is the overall density of the sample,  $\rho_a$  is the density of amorphous phase which was taken to be  $854 \text{ kgm}^{-3}$  [18], and  $\rho_c$  is the density of crystalline phase which was determined using

$$\rho_c = \phi_\beta \rho_{\beta c} + (1 - \phi_\beta) \rho_{\alpha c} \quad (4)$$

where  $\phi_\beta$  estimated using Eq. (1) was employed.

## 2.2 Crystallization process

The morphological feature and the growth rate of the spherulites as a function of time were examined using a polarized optical microscope during the isothermal crystallization process. A polarized optical microscope (OLYMPUS, B201) fitted with an automated hot stage was used. The hot stage (METTLER TOLEDO, FP82HT) was held at a steady temperature to  $\pm 0.2 \text{ K}$  by a proportional controller. The film including  $\beta$ -nucleators was sandwiched between a microscope slide and a cover glass, heated to  $483 \text{ K}$  and kept at this temperature for  $10 \text{ min}$  to melt the crystallites completely. Then the samples were rapidly quenched to a given crystallization temperature  $T_c$  and allowed to crystallize isothermally. In **Figure 1**, the growth rates of  $\alpha$ - and  $\beta$ -spherulites are plotted against the inverse of temperature. The growth rates increased with decreasing temperature over the whole experimental temperature ranges. **Figure 1** reveals that the difference between the two growth rates decreases with increasing temperature as shown by previous studies [6] and the growth rate of the  $\beta$ -spherulites exceeds that of the  $\alpha$ -spherulite below  $410 \text{ K}$  which is slightly lower than  $413\text{--}414 \text{ K}$  determined by Shi et al. [19] and Varga [20]. This strongly suggests that the  $\beta$ -spherulites are relatively larger than the  $\alpha$ -spherulites in iPP materials containing both phases prepared under usual conditions.

According to several kinetic theories [21–23], the growth rate  $G$  can be expressed by

$$G = G_0 \exp(-\Delta H/RT_c) \exp(-K_g/T\Delta Tf) \quad (5)$$

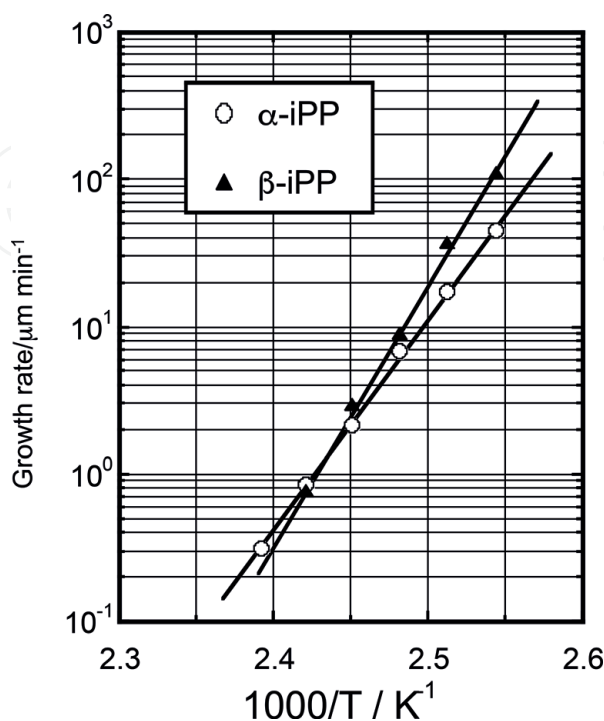


**Figure 1.** Temperature dependence of growth rate of  $\alpha$ - and  $\beta$ -spherulites.

where  $G_0$  is a pre-exponential factor that is independent of temperature,  $\Delta H$ , which is equal to 6.28 kJ/mol and corresponds to the activation energy of chain motion in the melt [22],  $\Delta T = T_m^0 - T$  ( $T_m^0$  is the equilibrium melting temperature),  $f = 2T_c / (T_m^0 + T_c)$  is a correcting factor, and  $K_g$  is the nucleation constant in which the crystallization mechanism is divided into three regions, Regimes I, II and III, depending on the crystallization temperature and given by

$$K_{g(I)} = 2K_{g(II)} = K_{g(III)} = 4b_0\sigma\sigma_e T_m^0 / \Delta h_f k_B \quad (6)$$

where  $\Delta h_f$  is the heat of fusion,  $b_0$  is the thickness of the new layer,  $\sigma$  is the lateral surface free energy,  $\sigma_e$  is the fold surface free energy, and  $k_B$  is the Boltzmann constant. According to Hoffman et al. [21], the surface free energy can be estimated using

$$\sigma = \Delta h_f \frac{a_0 l_b}{l_u C_\infty} \quad (7)$$

where  $a_0$  is the width of new layer,  $l_b$  (=0.154 nm) is the bond length,  $l_u$  (=0.1084 nm) is the projection length per atom, and  $C_\infty$  (=5.7) is the characteristic ratio [23]. The essential parameters for the kinetic study of  $\beta$  crystallization [19] are  $T_m^0 = 449$  K,  $\Delta h_f = 177$  MJm<sup>-3</sup>,  $a_0 = 0.636$  nm, and  $b_0 = 0.551$  nm. As a result, the surface energy  $\sigma$  was estimated to be  $1.4 \times 10^{-4}$  J m<sup>-2</sup>.

Using Eq. 6,  $\log G + \Delta H/2.303RT_c$  was plotted against  $1/T\Delta Tf$  as shown in **Figure 2**. Two linear parts corresponding to Regime II and Regime III were obtained: the change in the slope occurs at 401 K, which is in the range (396–403 K) published in the literature [1], and the slope ratio is 1.74. It was estimated that  $\sigma_e = 2.68\text{--}3.08 \times 10^{-2}$  J m<sup>-2</sup> from the slopes using  $\sigma$  of  $1.4 \times 10^{-4}$  J m<sup>-2</sup>. The work of chain folding  $q$  can be derived from the fold surface energy given by  $q = 2\sigma_e a_0 b_0$ . Consequently, the value of  $q$  for the  $\beta$ -phase was estimated to be 11–13 kJ/mol, which is about half the value (28 kJ/mol) for the  $\alpha$ -phase given by Shi et al. [19].

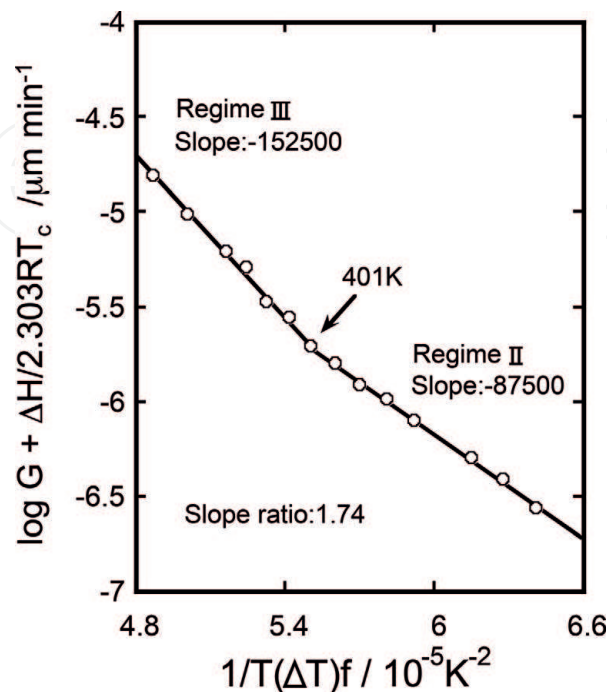


**Figure 2.**  
 Regime analysis of the growth rate of the  $\beta$ -spherulites.

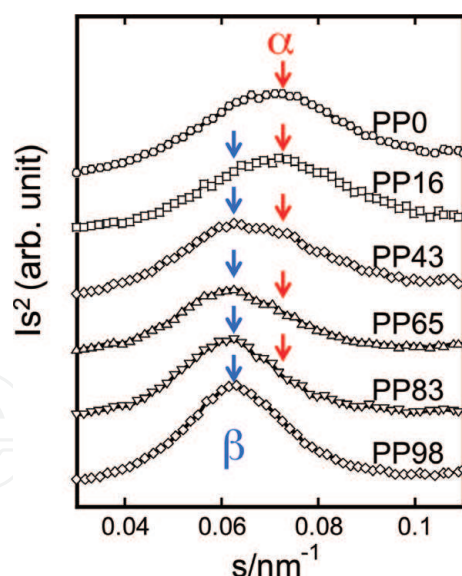


**Figure 3.** Lorentz-corrected SAXS patterns of iPP samples having different  $\beta$ -contents with a fixed crystallinity.

### 2.3 Crystalline morphology

The small angle X-ray scattering (SAXS) measurement was performed with a point-focusing optics and a one-dimensional position-sensitive proportional counter (PSPC) with an effective length of 10 cm. The CuK $\alpha$  radiation supplied by a MAC Science M18X generator operating at 40 kV and 30 mA was used throughout. The distance between the sample and PSPC was about 40 cm. The geometry was further checked using a chicken tendon collagen, which gives a set of sharp diffraction spots corresponding to 65.3 nm.

From the volume fraction of the crystals  $\chi_V$ , and SAXS long period  $L_p$ , the lamellar crystal thickness  $L_c$  and amorphous layer thickness  $L_a$  can be determined, assuming a two-phase model, from the following relationship:

$$L_c = \chi_V L_p, \quad L_a = (1 - \chi_V) L_p \quad (8)$$

**Figure 3** shows the Lorentz-corrected SAXS intensities plotted against magnitude of scattering vector  $s$  ( $= 2/\lambda \sin\theta$ ) where  $2\theta$  is the scattering angle and  $\lambda$  is the X-ray wavelength ( $= 0.1542$  nm). The maximum point in the SAXS curves yields the average long period. The  $s$  value of  $\alpha$ -PP (or PP0) was around  $0.072$  nm $^{-1}$ , and the  $s$  value of  $\beta$ -iPP (or PP98) was around  $0.0625$  nm $^{-1}$ , indicating that the long period  $L_p$  of  $\beta$ -iPP is greater than that of  $\alpha$ -iPP. The iPP samples with both modifications have two SAXS peaks corresponding to the  $\alpha$ -phase peak near  $0.072$  nm $^{-1}$  and  $\beta$ -phase peak near  $0.0625$  nm $^{-1}$ . This strongly suggests that the modified iPP samples with the  $\alpha$ - and  $\beta$ -spherulites coexist but no co-crystallization of  $\alpha$ -phase and  $\beta$ -phase crystals takes place. The specific long periods for  $\alpha$ -phase and  $\beta$ -phase were about 14 and 16 nm.

### 3. Tensile deformation

The sample specimens were cut into a dumbbell shape having a gauge length of 10 mm. The tensile strain was calculated from the ratio of the increment of the length between the clamps to the initial gauge length. The tensile stress was determined by dividing the tensile load by the initial cross section. The stress-strain

curves at room temperature were measured at a constant crosshead speed of 20 mm/min.

**Figure 4a** shows the overall stress–strain curves for all the samples with various  $\beta$ -phase contents at the same crystallinity. The ultimate tensile elongation markedly increases with increasing the  $\beta$ -phase content, and the  $\beta$ -iPP (PP98) has higher drawability than  $\alpha$ -iPP (PP0). The  $\beta$ -iPP is elongated more gradually with ambiguous necking as compared to  $\alpha$ -iPP, which is elongated with obvious necking.

As seen in **Figure 4b**, the initial elastic strain domain is surprisingly insensitive to the change in the composition of the crystalline phase at a fixed crystallinity. Thus, Young’s modulus was constant and completely independent of the  $\beta$ -phase content (see **Figure 5**). This phenomenon is responsible for the strain concentration in the amorphous region [24] because the amorphous phase in iPP is rubberlike at room temperature and the mechanical modulus of the amorphous phase is considerably lower than those of  $\alpha$ - and  $\beta$ -phase crystals. Consequently, before yielding, the deformation of the semicrystalline polymers is dominated by the deformation of the amorphous phase, indicating that the initial elastic region depends mainly on the crystallinity.

The elasticity limits where the actual stress–strain curves for the  $\beta$ -modified iPP samples are deviated from the linear elastic behavior were around 0.1 strain as shown in **Figure 4b**. The deviation may be due to the onset of microscopic plastic

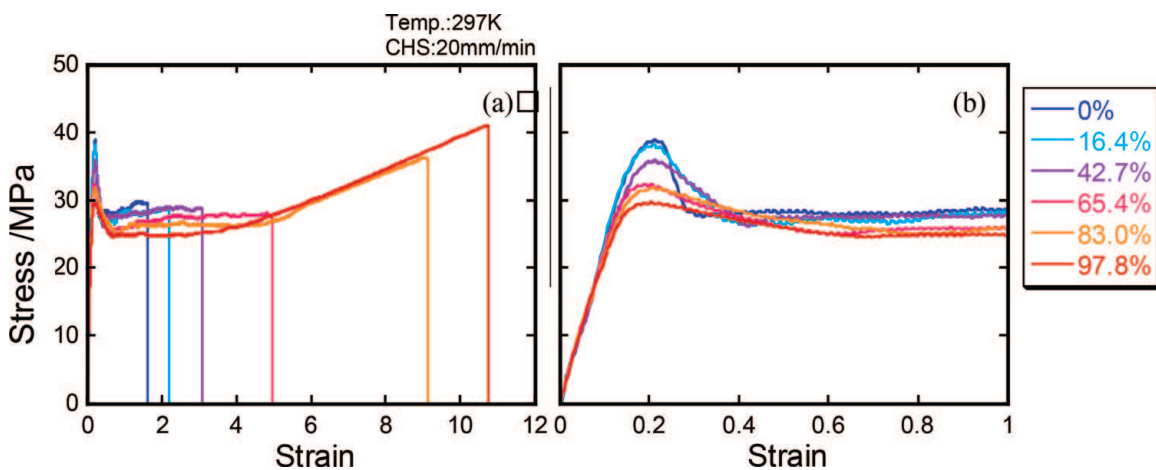


**Figure 4.** Stress–strain curves of iPP samples having different  $\beta$ -contents with a fixed crystallinity. (a) Overall curves and (b) their magnification in the initial strains.

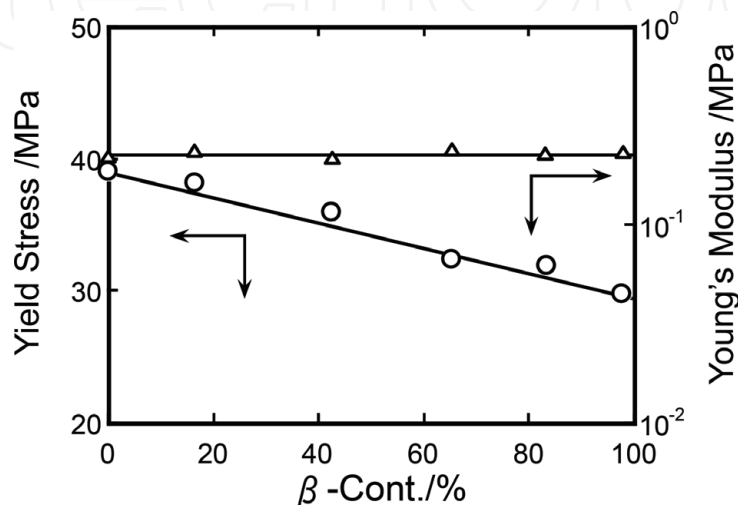


**Figure 5.** Yield stress and Young’s modulus plotted against the  $\beta$ -contents for the  $\beta$ -nucleated iPP.

deformation resulting from the lower packing density of the  $\beta$ -phase. The main differences in the stress-strain curves exist in the yield region. In this region, the macroscopic structural transformation from a spherulitic structure to microfibrils takes place.

The yield process was found to become broader as the  $\beta$ -phase content increases, and the yield stress linearly decreases with increasing  $\beta$ -phase content (see - **Figure 5**). This is relevant to the early and more gradual activation of plastic processes in the  $\beta$ -phase as compared to  $\alpha$ -phase because of the higher molecular mobility in the  $\beta$ -phase at the same temperature. This demonstrates that the plastic behavior is much more sensitive to the nature of the crystalline phase. In addition, the yield peak in the stress-strain curves broadens, and the neck region is more ambiguous as the  $\beta$ -phase increases. As mentioned before, the  $\beta$ -phase crystals have a lower cohesive force than the  $\alpha$ -phase crystals, which is also reflected by their lower melting temperature and lower density. The lower cohesive force leads to easier slipping of the lamellar chains, resulting in a lower yield stress. Furthermore, as shown in **Figure 6**, the yield energy, which is defined as the energy dissipated for yielding to take place, linearly increases with increasing  $\beta$ -phase content, and all data almost fall on the solid line, which can be calculated according to the simple mixture law as follows:

$$U_Y = \phi_\beta U_{\beta Y} + (1 - \phi_\beta) U_{\alpha Y} \quad (9)$$

Here  $U_Y$  is the yield energy (resilience), which was estimated from the area under the stress-strain plot from the origin to the stress drop, and  $U_{\beta Y}$  and  $U_{\alpha Y}$  are the yield energies of  $\beta$ -iPP and  $\alpha$ -iPP, respectively.

To obtain better insights into the plastic behavior of the crystalline component, the WAXD experiments were carried out at room temperature during tensile tests. The direction of the incident beam was perpendicular to the plate surface of the specimens. **Figure 7** shows the WAXD patterns of  $\alpha$ -iPP (PP0) and  $\beta$ -iPP (PP98). The WAXD patterns of the undrawn specimens of PP0 and PP98 are shown in **Figures 7a** and **d**, respectively. The patterns of iPP0 stretched at a strain of 0.4 and PP98 stretched at a strain of 0.8, in which both stretched samples are in the post-yielding region, are shown in **Figures 7b** and **e**, respectively, and those of both specimens at the final failure point are shown in **Figures 7c** and **f**, respectively. The Debye rings of the (300) and (030) reflections of the  $\beta$ -phase crystals remain in the

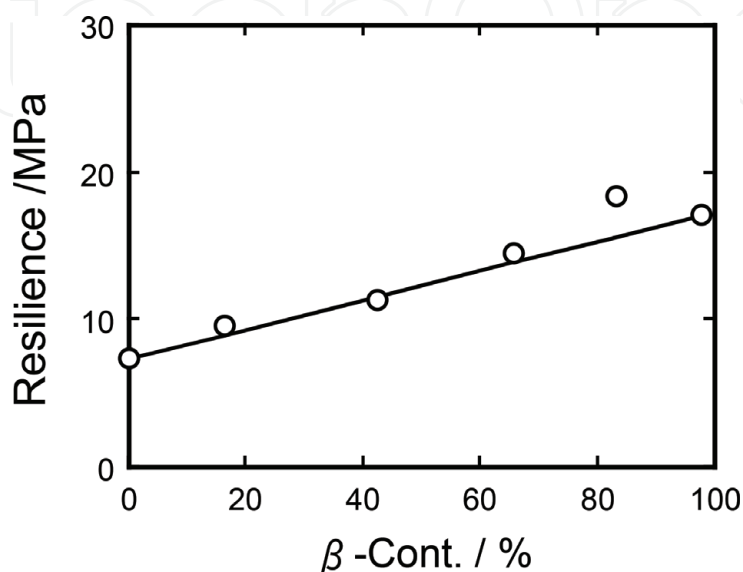


**Figure 6.** Yield energy (resilience) plotted against the  $\beta$ -contents for the  $\beta$ -nucleated iPP.

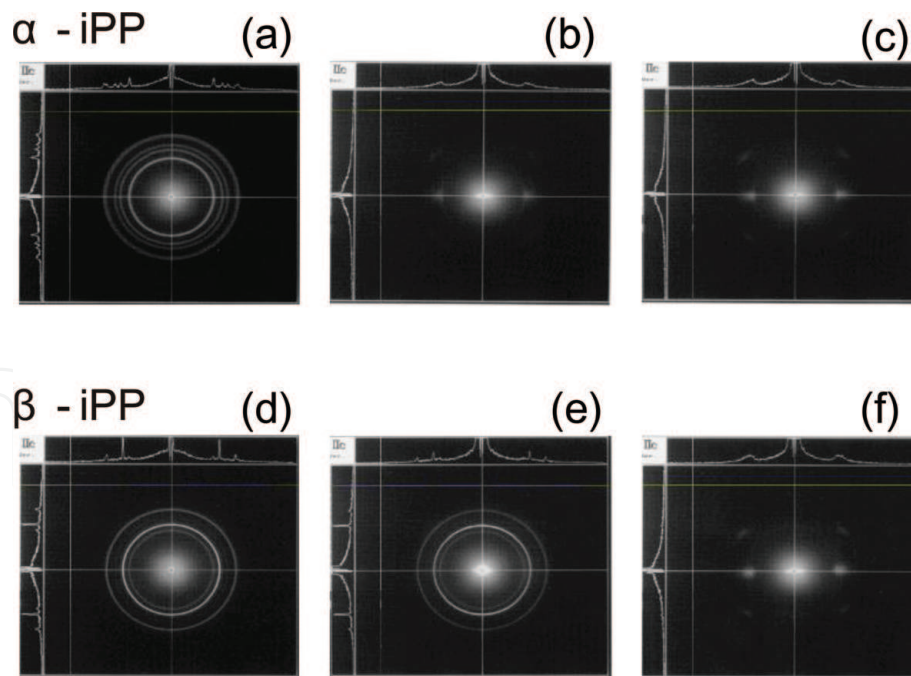


**Figure 7.** Small angle X-ray diffraction patterns of  $\alpha$ - and  $\beta$ -iPP samples: (a) original  $\alpha$ -iPP, (b) stretched  $\alpha$ -iPP at a strain of 0.4 (neck region), (c) stretched  $\alpha$ -iPP at the failure point, (d) original  $\beta$ -iPP, (e) stretched  $\beta$ -iPP at a strain of 0.8 (neck region), and (f) stretched  $\beta$ -iPP at the failure point.

PP98 sample deformed up to the post-yielding region (see **Figure 7e**), and they are scarcely oriented even in the initial necking region. In contrast to PP98, PP0 exhibits the reflections of the  $\alpha$ -phase concentrated in the perpendicular direction to the elongation even in the post-yielding and necking regions. This pattern is almost the same as the typical profile of the iPP specimens at the final failure point, indicating that  $\alpha$ -iPP attains the final  $c$ -axis orientation of crystals after yielding. In addition, it should be noted here that there is no clear difference in the orientation pattern at the final failure point between PP98 and PP0. The strain induced  $\beta \rightarrow \alpha$  transition on tensile drawing has been reported by several authors [25–29]. In the present work, there is no evidence for the occurrence of a  $\beta \rightarrow \alpha$  transition as seen in **Figure 7f**, but the final orientation morphology of PP98 appears to be the same as that of PP0. The reflections showing the attainable final orientation exist between 14 and 16°, suggesting the assignment of smectic form as demonstrated by Turner-Jones et al. [12] and Shi et al. [8].

#### 4. Deformation of isolated spherulites

According to our previous studies [30, 31] concerning the yield behavior of typical spherulitic polymers such as PE and  $\alpha$ -iPP, several lamellae tend to cluster into bundles with tie molecules, where these are separated from one another by the amorphous regions and the lamellar clusters constituting of spherulites act as deformation units. The lamellar clusters are bridged by the inter-cluster or intercrystalline links, as proposed by Keith-Padden et al. [32], thus acting as stress transmitters. The stacked lamellae or lamellar clusters are fragmented into cluster units or blocks at the yield point, resulting in a stress drop. Beyond the yield point, the plastic deformation involves the rotation of the cluster units and the sliding of stacked lamellae inside each cluster units, and the fragmented cluster units are rearranged into microfibrils in the necking region [33]. The continuous structural transformation corresponds to the neck propagation. In the case of  $\beta$ -spherulitic iPP

showing a broad yield process, the lamellar clusters disintegrate accompanied by sliding crystalline stems and chain slip inside the crystalline lamellae. Consequently, the fragmentation of lamellae and/or lamellar clusters hardly occurs. These differences in yielding mechanism between  $\alpha$ - and  $\beta$ -spherulitic iPPs are due to the differences not only in the cohesive force between crystalline chains but also in the spherulite morphology.

**Figure 8** shows an atomic force microscopy (AFM) micrograph of the morphology of the  $\beta$ -form iPP spherulites prepared in this work. The morphology is significantly different from the typical spherulite morphology of  $\alpha$ -phase iPP. This spherulite seems to be type III according to Norton and Keller's classification [34] because there is no lamellar twisting within the spherulites. The embryo  $\beta$ -spherulites consist of parallel stacked lamellae. This type of spherulite is referred to as a sheaflike structure. Shi et al. [19] reported that the  $\beta$ -spherulites develop initially as rodlike structures and then by branching of the lamellae, finally evolving into sheaflike structures. In this case, the spherulite is formed from one crystal via a unidirectional growth mechanism. The spherical shape is attained through continuous branching and fanning via the intermediate stage of sheaves. However, the  $\alpha$ -spherulites consist of an aggregate of chain-folded lamellae growing from a central point (nucleus). This is referred to as an acicular structure. Both structural models of  $\alpha$ - and  $\beta$ -spherulites are shown in **Figure 9**.

It is likely that the spherulite morphology plays a central role in controlling the plastic deformation and tensile behavior of both PE and iPP materials. The mechanical responses to tensile yielding and the deformation process are considered to be fundamentally different between  $\alpha$ - and  $\beta$ -spherulites. Tensile deformation of  $\alpha$ -iPP materials is accompanied by necking process, in which the initial isotropic

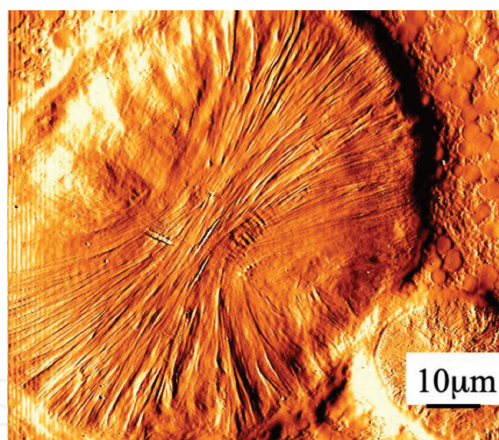


**Figure 8.**  
AFM pictures of a  $\beta$ -spherulite.

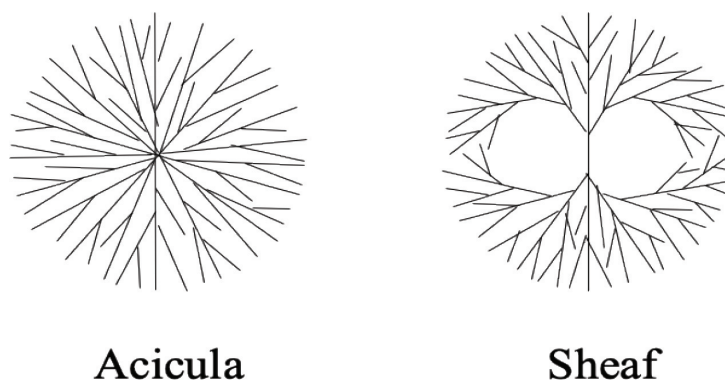


**Figure 9.**  
Illustrations of lamellar arrangement of  $\alpha$ - and  $\beta$ -spherulites.

spherulite structure is converted into a highly oriented one. On the other hand, the  $\beta$ -iPP exhibits broader yield peaks without obvious necking formation and has a lower yield strength than that of  $\alpha$ -iPP. Furthermore, the  $\beta$ -iPP specimen began to be whitened with further extension, whereas the  $\alpha$ -iPP exhibited partial stress whitening beyond yielding. This stress whitening seems to be caused by the formation of numerous voids after yielding [35].

Previously, we reported a method for preparing a thin film with huge isolated spherulites embedded in a soft (smectic) matrix [36]. The deformation mechanism of spherulites can be examined from the direct observation of the stretched film on the polarized optical microscope. Thus, we mounted the manual stretcher on the optical microscope to observe the deformation process of the isolated spherulites.

**Figure 10a** shows the optical microscopic pictures of an isolated  $\alpha$ -spherulite. A few arc-shaped cracks rapidly appeared in the polar zone in the initial stages of

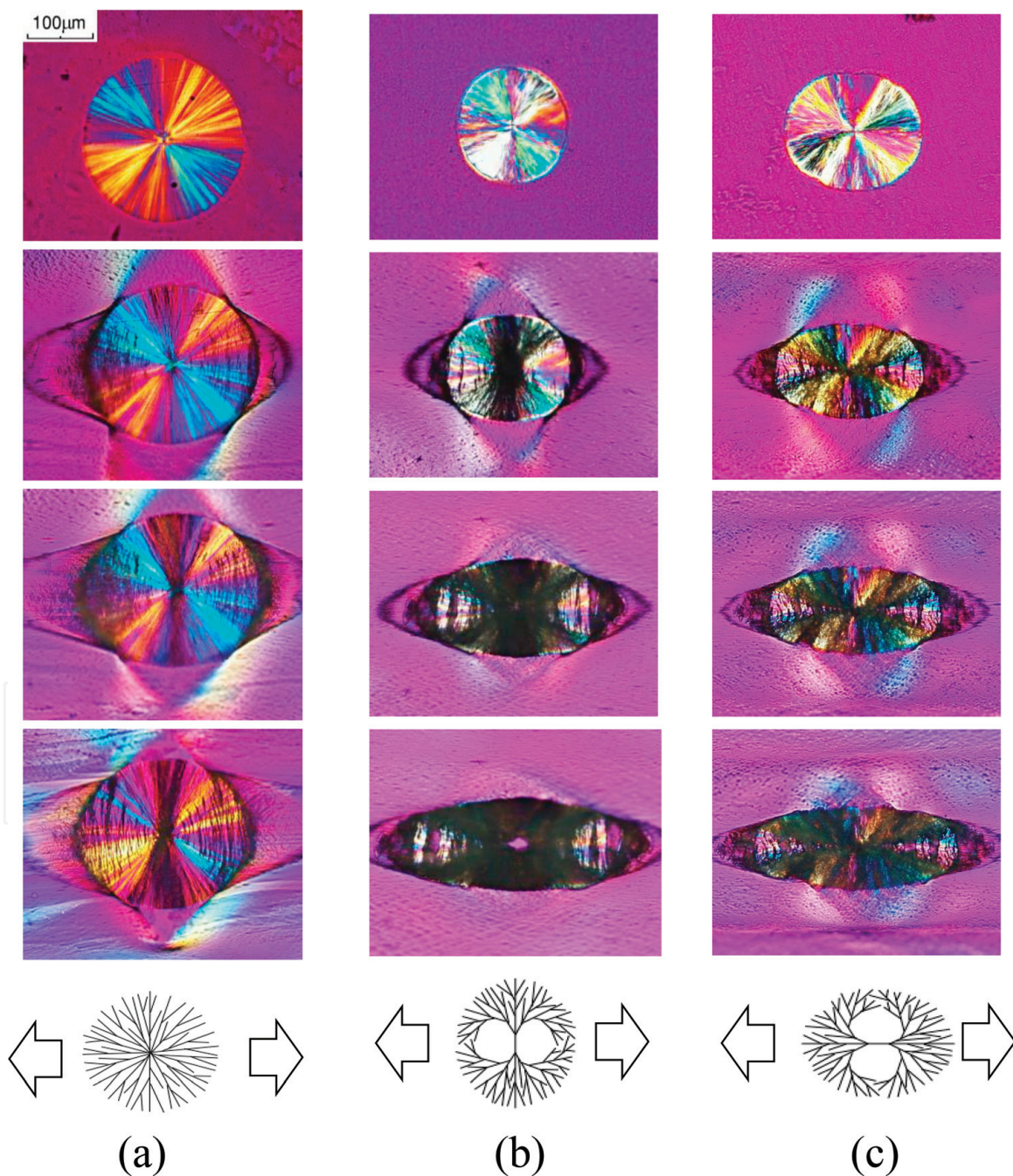


**Figure 10.** Polarized optical microscopic pictures of (a) uniaxial stretching of an isolated  $\alpha$ -acicular spherulite, (b) uniaxial stretching perpendicular to the sheaf axis of an isolated  $\beta$ -sheaf spherulite, and (c) uniaxial stretching parallel to the sheaf axis of an isolated  $\beta$ -sheaf spherulite.

stretching. With increasing strain, the arc-shaped cracks developed in the polar zone and proceed from the outer to the inner portions of the spherulite. Subsequently, radial craze-like fractures began to form in the equatorial region perpendicular to the stretching axis, and then the radial crazing progressed along with the spherulite radius, resulting in the evolution of large dark bands in the equatorial region. The evolution of the dark bands is related to the yield process as demonstrated previously by Nitta et al. [36]. It should be noted here that the deformation mechanism of  $\alpha$ -spherulites is isotropic because crystalline lamellae within  $\alpha$ -spherulites radiate from a common center and the crystalline lamellae aggregate with spherical symmetry. Unlike the  $\alpha$ -spherulite,  $\beta$ -spherulites are sheaflike type of spherulites with a spherical asymmetry (see **Figure 9**). As shown in **Figure 10b** and **c**, the deformation behavior of the  $\beta$ -spherulite depends largely on the stretching direction with respect to the sheaf axis. In the case of the  $\beta$ -spherulites, when drawn perpendicular to the sheaf direction, the radial crazing preferentially appeared in the equatorial zone along the sheaf axis, and then the dark crazing zone developed further with increasing strain. Finally, a hole appeared in the center of the deformed spherulite, indicating that the deformation is concentrated perpendicular to the stacked lamellae located in the center of the spherulite. On the other hand, when drawing along the sheaf axis, the spherulite was deformed into an ellipsoid accompanied by the formation of crazed cracks, and there is no clear strain concentration.

It was found that the strength of the  $\beta$ -spherulite is anisotropic and depends on the direction of the embryo or parallel stacked lamellae in the center of the spherulite. When the  $\beta$ -spherulites were subjected to stress perpendicular to the sheaf axis (see **Figure 10b**), obvious deformation bands generated preferentially near the equatorial zone within the uniaxially deformed spherulites. According to previous theoretical [37, 38] and experimental results [39], the equatorial region, particularly the center of the spherulites, is subjected to higher strains and stresses as compared to the polar region. Consequently, interlamellar separation is likely to occur near the equatorial plane of the stacked sheaflike lamellae because the sheaf direction is perpendicular to the loading direction. As the strain increased, separation of the sheaf-lamellae continued, and more deformation bands and crazes generated preferentially near the equatorial zone of the deformed spherulites. In the final stage, holes or local disintegration appeared near the center of the deformed spherulites. This lamellar separation was accompanied by massive voiding at the onset of the formation of a microporous structure, which is preferential for the applications of  $\beta$ -phase iPP [29, 40]. On the other hand, when the  $\beta$ -spherulite was stretched in the growth direction of the embryo sheaf (see **Figure 10c**), there was no obvious deformation bands around the equatorial zone. Thus, intralamellar deformation is likely to take place for the sheaf-lamellae under uniaxial tension because the sheaf-lamellae are parallel to the loading direction. Considering that the intralamellar stretching of the sheaf-lamellae involves the unfolding of chains, leading to local necking or sliding, the intralamellar stretching of sheaf-lamellae strongly resists deformation compared to the interlamellar separation; thus, no localized deformation bands appeared near the equatorial zone.

As well-known, the  $\beta \rightarrow \alpha$  transformation occurs on heat treatment. The film having isolated  $\beta$ -spherulites was heated up to 433 K at a rate of 2 K/min and then quenched in an ice-water bath. This treatment allows the recrystallization into  $\alpha$ -modification within the isolated  $\beta$ -spherulites. The arrangement of the crystalline lamellae in the  $\alpha$ -spherulites prepared by the  $\beta \rightarrow \alpha$  transformation is a sheaflike structure, which is different from the usual  $\alpha$ -spherulites showing an acicular structure. Thus, the sheaflike spherulite prepared by the  $\beta \rightarrow \alpha$  transformation process is a new type of  $\alpha$ -spherulite. As shown in **Figure 11**, the sheaflike

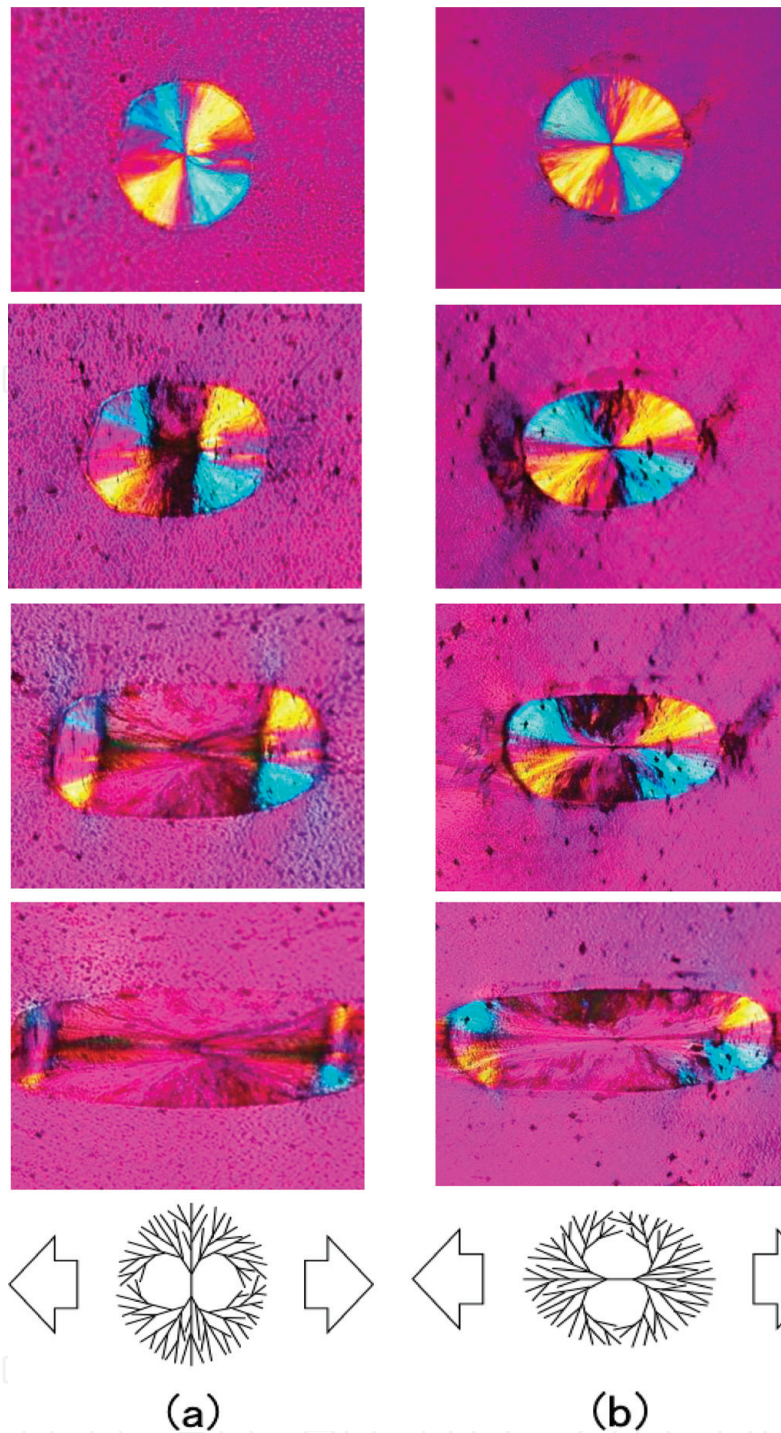


**Figure 11.** Polarized optical microscopic pictures of (a) uniaxial stretching perpendicular to sheaf axis of an isolated  $\alpha$ -sheaf spherulite and (b) uniaxial stretching parallel to sheaf axis of an isolated  $\alpha$ -sheaf spherulite.

$\alpha$ -spherulite is optically negative, indicating that there are no traces of a cross-hatched structure within the  $\beta$ -spherulites.

The deformation behavior of the sheaflike  $\alpha$ -spherulite was also anisotropic and significantly different from that of the acicular type of  $\alpha$ -spherulite as shown in **Figure 10**. When the axis of the sheaf was transverse to the loading direction, the deformation bands appeared obviously along the sheaf axis, and then the further deformation extended the highly oriented and deformed zone in the equatorial region of the deformed spherulite. The uniaxially deformed spherulite is clearly divided into two parts: one being nearly undeformed and another being considerably deformed. The nearly undeformed sections are jointed by the transition zone that propagates in the stretching direction. The interlamellar separation of stacked

sheaf-lamellae in the equatorial zone was initiated in the first stage of deformation, and then the separation of the sheaf-lamellae continues, and more deformation bands proceeded as the strain was further increased. On the other hand, when the sheaf axis was in the draw direction (see **Figure 11b**), the spherulite was initially deformed to an ellipse of similar shape to that expected for affine deformation. This is because its equatorial region is tougher because the lamellae parallel to the stretching direction more strongly resist deformation than the lamellae perpendicular to the loading direction as mentioned in the discussion of  $\beta$ -spherulite deformation. Subsequent deformation caused micro-necking in such a way that the traces of the sheaf structure remain in the center portion of the spherulite. The sheaf-lamellae located perpendicular to the loading direction are brittle, whereas the sheaf-lamellae located parallel to the loading direction are tougher or ductile. This anisotropic deformation behavior is quite different from the isotropic deformation of acicular  $\alpha$ -spherulites, but it is similar to those of sheaf  $\beta$ -spherulites as well as isolated PE spherulites, as shown by Lee et al. [41]. This is plausible because PE spherulite is sheaflike.

It has been long recognized that the deformation of crystalline polymers must be considered in terms of various structural parameters such as crystallinity, lamellar thickness or long period, and spherulite size. However, the present results imply that deformation behavior and mechanical response of bulk iPP materials are affected not only by these structural factors but also by the morphological texture within spherulites.

## 5. Effects of spherulite morphology on tensile properties

To investigate the effects of the lamellar organization within the spherulites on the tensile properties of bulk iPP sheets,  $\alpha$ -modified iPP samples were prepared by

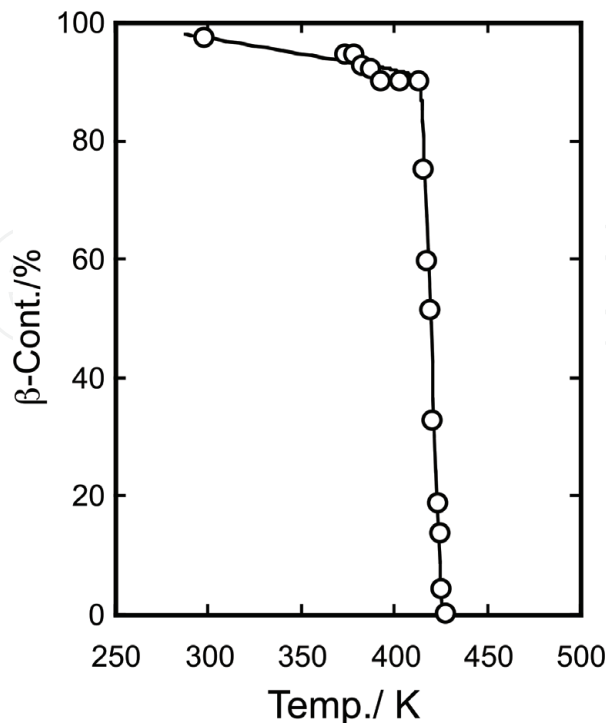


**Figure 12.**

*Dependence of  $\beta$ -contents of  $\beta$ -nucleated iPP on the heat-treatment temperature.*

the heat treatment of  $\beta$ -iPP (PP98) sheets. The PP98 sheets were heated at a 2 K/min and kept for 300 min at a fixed temperature. The  $\beta$ -phase contents are plotted against the fixed temperature in **Figure 12**. The  $\beta \rightarrow \alpha$  transformation occurs at around 413 K, and the  $\beta$ -iPP was completely transformed into the  $\alpha$ -phase above 427 K. It should be noted here that the thus-prepared iPP sheets contain sheaf type of spherulites. Consequently, we obtained three types of iPP sheets having a fixed crystallinity of around 73%, for example, the  $\alpha$ -iPP sheets showing acicular spherulites, the  $\alpha$ -iPP sheets showing sheaflike spherulites, and the  $\beta$ -iPP sheets showing sheaflike spherulites. Here, we have referred to these samples as  $\alpha$ -acicular,  $\alpha$ -sheaf, and  $\beta$ -sheaf.

**Figure 13** shows the stress-strain curves measured at various temperatures for  $\alpha$ -acicular,  $\alpha$ -sheaf, and  $\beta$ -sheaf sheets. At all temperatures, the stress-strain curves in the initial elastic strain domain were almost the same for these three samples. This is plausible because the crystallinities of these samples are almost equal. This also indicates that Young's modulus is dominated by the bulk crystallinity and is almost independent of the lamellar morphology of the spherulites and of the crystal modification. In addition, the  $\alpha$ -acicular iPP sample is in more brittle manner than the  $\alpha$ -sheaf and the  $\beta$ -sheaf iPP samples and broke around the yield peak except at 380 K. This indicates that the plastic deformation is much more sensitive to the change of the spherulite texture than to crystalline modification. This corroborates the previous results that the deformation behavior of isolated  $\beta$ -sheaf and  $\alpha$ -sheaf spherulites is similar and significantly different from that of the  $\alpha$ -acicular spherulites. Moreover,  $\beta$ -spherulites show a greater resistance to break when the strain direction is almost parallel to the sheaf axis. Interestingly, the yield strengths in  $\alpha$ -acicular and  $\alpha$ -sheaf iPPs are almost the same, although

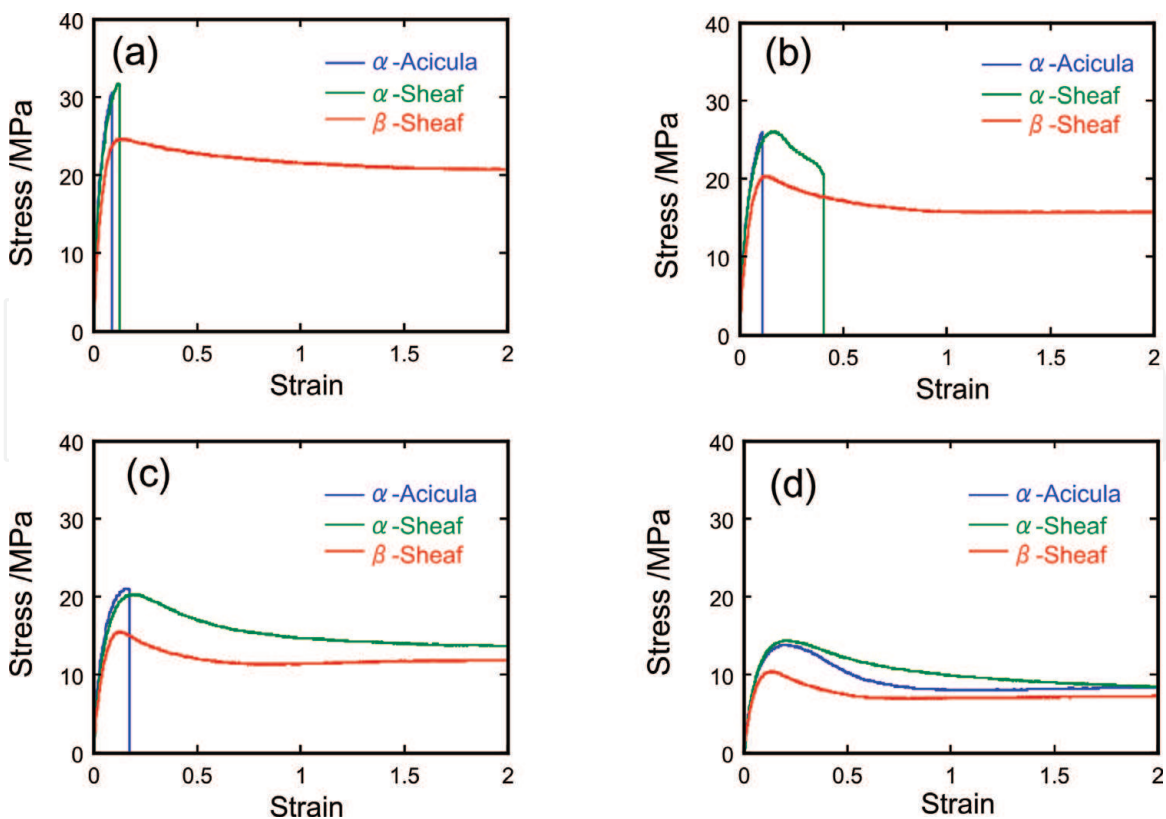


**Figure 13.** Comparison of stress-strain curves of spherulitic iPP sheets with a fixed crystallinity:  $\alpha$ -acicular spherulites (blue),  $\alpha$ -sheaf spherulites (green), and  $\beta$ -sheaf spherulites (red).

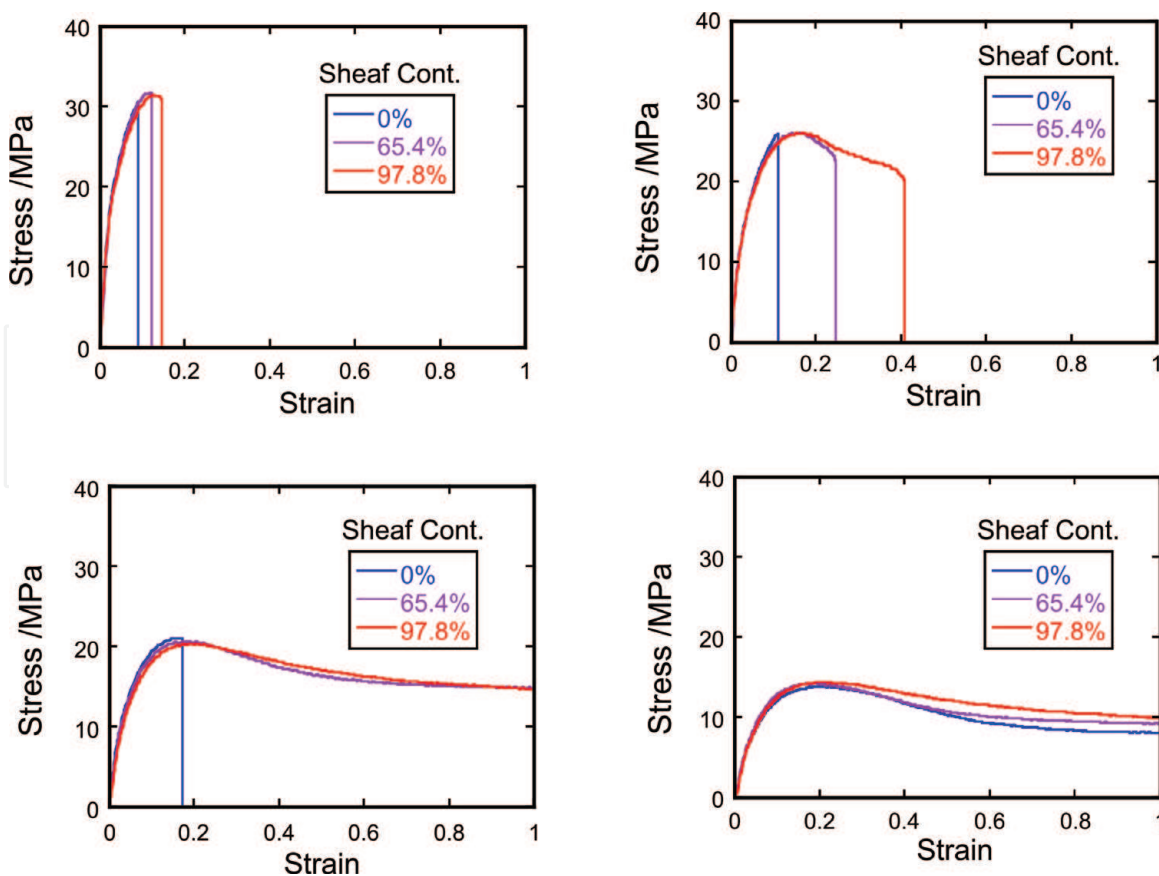


**Figure 14.** Comparison of stress-strain curves of  $\alpha$ -spherulitic iPP samples with different contents of sheaflike spherulites.

larger than that of the  $\beta$ -sheaf iPP. This indicates that the yield strength is much more sensitive to crystal phase modification than to the lamellar arrangement of the spherulites. The reduced yield stress of  $\beta$ -sheaf iPP compared to those of the  $\alpha$ -acicular and  $\alpha$ -sheaf iPPs is associated with the greater chain mobility in the  $\beta$ -phase crystals. The lower packing density of the  $\beta$ -phase is accompanied by the reduced stem interactions in the  $\beta$ -crystalline lamellae as compared to the  $\alpha$ -lamellae, leading to the lower yield stress of the  $\beta$ -phase compared to that of the  $\alpha$ -phase. An additional factor reducing the lamellar strength is the crystallographic symmetry of the hexagonal  $\beta$ -phase, which provides three equivalent glide planes.

To confirm these conclusions, we compared the stress-strain behaviors measured from 320 to 380 K for  $\alpha$ -spherulitic iPP sheets with different amounts of sheaflike spherulites which were prepared by tempering the iPP samples with the different amount of  $\beta$ -spherulites. Note here that these iPP sheets have a fixed crystallinity of about 74%. As a result,  $\alpha$ -spherulitic iPP sheets having various sheaflike spherulite contents with constant crystallinity were prepared. **Figure 14** also shows that the ductility enhances as the content of sheaf spherulites increased, whereas the yield strengths of all sheets are the same and almost insensitive to the lamellar arrangement of the spherulites.

## 6. Summary

Based on our investigation of the tensile properties of  $\alpha$ -iPP and  $\beta$ -modified iPP, in which all the other structural parameters, such as overall crystallinity and spherulite size, were controlled, the following conclusions can be drawn:

- (1) The stress-strain curves in the initial elastic strain region are dominated by the effects of crystallinity but are almost insensitive to changes in the crystal phases, as well as to the lamellar arrangements of spherulites.
- (2) The yield strength is more sensitive to the crystal modification than the lamellar arrangement of spherulites, and  $\alpha$ -iPP shows a higher yield stress than  $\beta$ -modified iPP.
- (3) The plastic deformation process of the spherulites is sensitive to the lamellar arrangement of spherulites. The sheaflike spherulites are more ductile than the acicular spherulites and exhibit anisotropy in their plastic properties. The improved drawability and ductility of  $\beta$ -iPP compared with  $\alpha$ -iPP is thus associated with the enhanced toughness resulting from multiple deformation processes in the sheaflike spherulites.

IntechOpen

### Author details

Koh-hei Nitta\* and Tsutomu Takashima  
Institute of Science and Engineering, Kanazawa University, Kanazawa, Japan

\*Address all correspondence to: [nitta@se.kanazawa-u.ac.jp](mailto:nitta@se.kanazawa-u.ac.jp)

### IntechOpen

© 2018 The Author(s). Licensee IntechOpen. This chapter is distributed under the terms of the Creative Commons Attribution License (<http://creativecommons.org/licenses/by/3.0>), which permits unrestricted use, distribution, and reproduction in any medium, provided the original work is properly cited. 

## References

- [1] Karger-Kocsis J. Polypropylene Structure, Blends and Composites. Vol. 1. London: Chapman and Hall; 1995
- [2] Padden FJ Jr, Keith HD. Journal of Applied Physics. 1959;**30**(10): 1479-1484
- [3] Lovinger AJ, Chua JO, Gryte CC. Journal of Polymer Science Part B: Polymer Physics. 1977;**15**(4):641-656
- [4] Varga J. Karger-Kocsis. Journal of Polymer Science Part B: Polymer Physics. 1996;**34**:657-670
- [5] Varga J, Ehrenstein GW. Polymer. 1996;**37**(26):5959-5963
- [6] Varga J. Crystallization, Melting and Supermolecular Structure of Isotactic. In: Karger-Kocsis J, editors. Polypropylene: Structure, Blends, and Composites. Vol. 1. London: Chapman and Hall; 1995. pp. 56-115
- [7] Varga J, Mudra I, Ehrenstein GW. Journal of Applied Polymer Science. 1999;**74**(10):2357-2368
- [8] Shi G, Zhang X, Cao Y, Hong J. Makromolekulare Chemie. 1993;**194**(1): 269-277
- [9] Varga J, Breining A, Ehrenstein GW, Bodor G. International Polymer Processing. 1999;**14**(4):358-364
- [10] Kennedy MA, Peacock AJ, Mandelkern L. Macromolecules. 1994; **27**(19):5297-5310
- [11] Labour T, Gauthier C, Seguela R, Vigier G, Bomal Y, Orange G. Polymer. 2001;**42**(16):7127-7135
- [12] Turner Jones A, Aizlewood JM, Beckett DR. Makromolekulare Chemie. 1964;**75**:134-158
- [13] Somani RH, Hsiao BS, Nogales A, Fruitwala H, Srinivas S, Tsou AH. Macromolecules. 2001;**34**(17): 5902-5909
- [14] Keith HD, Padden FJ, Walter NM, Wyckoff HW. Journal of Applied Physics;**1959**(10):30, 1485-1488
- [15] Samuels RJ, Yee RY. Journal of Polymer Science Part A2. 1972;**10**: 385-432
- [16] Addink EJ, Beintema J. Polymer. 1961;**2**:185-193
- [17] Natta G, Corradini P. Nuovo Cimento. Suppl. 1960;**15**(S1):40-51
- [18] Newman S. Journal of Polymer Science, Polymer Physics Edition. 1960; **47**:111
- [19] Shi G, Zhang X, Qiu Z. Makromolekulare Chemie. 1992;**193**(3): 583-591
- [20] Varga J. Journal of Materials Science. 1992;**27**(10):2557-2579
- [21] Hoffmann JD, Miller RL. Macromolecules. 1988;**21**:3038-3051
- [22] Hoffmann JD. Polymer. Vol. 231982. pp. 656-670
- [23] Hoffmann JD, Miller RL. Polymer. 1997;**38**:3151-3212
- [24] Nitta KH, Yamaguchi N. Polymer Journal. 2006;**38**(2):122-131
- [25] Asano T, Fujiwara Y. Polymer. 1978; **19**(1):99-108
- [26] Fujiyama M. International Polymer Processing. 1999;**14**:3-9
- [27] Karger-Kocsis J, Varga J. Journal of Applied Polymer Science. 1996;**62**(2): 291-300

[28] Li JX, Cheung WL. *Polymer*. 1998;  
**39**(26):6935-6940

[29] Chen HB, Karger-Kocsis J, Wu JS,  
Varga J. *Polymer*. 2002;**43**(24):  
6505-6514

[30] Nitta KH, Takayanagi M. *Journal of  
Macromolecular Science, Part B:  
Physics*. 2003;**42**:107-126

[31] Takayanagi M, Nitta K, Kojima O.  
*Journal of Macromolecular Science, Part  
B: Physics*. 2003;**42**:1049-1059

[32] Keith HD, Padden FJ, Vadimsky RG.  
*Journal of Polymer Science Part A-2*.  
1966;**4**:267-281

[33] Kuriyagawa M, Nitta KH. *Polymer*.  
2011;**52d**:3469-3477

[34] Norton DR, Keller A. *Polymer*. 1985;  
**26**(5):704-716

[35] Varga J. *Journal of Macromolecular  
Science, Part B. Physics*. 2002;**41** (4-6),  
1121-1171

[36] Nitta KH, Takayanagi M. *Journal of  
Materials Science*. 2003;**38**(24):  
4889-4894

[37] Nitta KH. *Computational and  
Theoretical Polymer Science*;**1999**(1):9,  
19-26

[38] Wang TT. *Journal of Polymer  
Science Part B: Polymer Physics*. 1974;  
**12**(1):145-158

[39] Rodriguez-Cabello JC, Alonso M,  
Merino JC, Pastor JM. *Journal of Applied  
Polymer Science*. 1996;**60**:1709-1717

[40] Coulon G, Castelein G, G'Sell C.  
*Polymer*. 1996;**37**:2309

[41] Lee SY, Bassett DC, Olley RH.  
*Journal of Materials Science*. 2000;  
**35**(20):5101-5110